A Real Time Sliding Mode Control for a Wave Energy Converter based on a Wells Turbine

Oscar Barambones, José A. Cortajarena, José M. Gonzalez de Durana
and Patxi Alkorta
Automatic Control and System Engineering Departament
EUI de Vitoria. University of the Basque Country
Nieves cano 12. 1006 Vitoria. (SPAIN)
oscar.barambones@ehu.es

Abstract

Due to the nonlinear dynamics and uncertainties usually present in wave energy conversion systems, the efficiency of these devices can be enhanced employing a robust control algorithms. Wave energy converters are constructed using electric generators of variable velocity, like double feed induction generator (DFIG) since they may improve the system efficiency to generate power when compared to fixed speed generators. The main reason is that this generators with variable speed may adapt the speed of the turbine in order to maintain the optimal flow coefficient values which improves the efficiency of the Wells turbine. However, a suitable speed controller is required in these systems first in order to avoid the stalling phenomenon and second in order to track the optimal turbine reference velocity that optimizes the power generation.

In this paper a real time sliding mode control scheme for wave energy conversion systems that incorporate a Wells turbine and a DFIG is proposed. The Lyapunov stability theory is used to analyse the stability of this control scheme under parameter uncertainties and system disturbances. Next, the proposed control scheme is validated first by means of some simulation examples using the Matlab/Simulink software and second using a real-time experimental platform based on a dSPACE DS1103 control board.

Keywords: Wave power; Wave energy converters; Sliding mode control; Real-time control; DFIG (doubly-fed induction generator).

1. Introduction

Renewable energy sources (i.e. wind and solar energy) have acquired an increasing interest in the last decade due to the harmful contamination effects caused by the traditional sources of energy. Recently, the international community has also paid special attention to wave energy, which could supply a considerable part of the electricity demand of some countries [1]-[4].

When the wind blows on the surface of the ocean it causes the waves. In some locations, the wind blows consistently and with sufficient force to produce continuous waves along the shoreline. Since ocean waves contain tremendous energy potential, different wave power devices have been designed to extract their energy. Typically, these devices benefit from the surface motion of ocean waves or from pressure fluctuations below the surface [5]-[7]. In this study, an oscillating water columns (OWC) device [8], [9] is employed in order to extract the energy of the ocean waves into mechanical energy using a Wells turbine [10]-[12]. The mechanical energy harvested in OWC's is determined by wave height, wave speed, wavelength, and water density [13], [14]. However, the energy produced in these systems can be improved by means of the turbine rotational speed control because the turbine speed affects the hydrodynamic process of wave energy absorption [15]-[17].

The mechanism of the wave energy conversion systems follows an oscillating movement so the rotor velocity of the coupled electric generator is variable. These systems should incorporate an AC-AC converter in order to generate an electric power of constant voltage and frequency [18]. However in this configuration the converter should manage all the generated power and this fact present some lacks like the cost of the converters and the power lost in the conversion.

On the other hand the generation system could incorporate the doubly fed induction generator (DFIG) that is currently used by other power generation plants, for example the wind turbine systems, because it allows a variable turbine speed operation [19],[20].

The stator of the DFIG is directly connected to the grid and the rotor of the DFIG is connected to the grid using a variable frequency converter (VFC). The advantage of this configuration is that in order to get the total control of the generator, the VFC only have to manage a fraction of the nominal power, around 25%-30%. The VFC incorporates one voltage source located on the side of the grid called grid-side converter (GSC) and another voltage source located on the side of the rotor called rotor-side converter (RSC). These voltage source converters are connected back-to-back through a capacitor [21]-[23].

This kind of systems are habitually controlled using a vector control scheme and cascaded PI-current and power loops [24]. However the nonlinear dynamics and the uncertainties presented in these systems suggest the use of a more robust controller in order to improve the system performance.

In this sense, one option is to consider the sliding mode control (SMC) because this kind of controller presents a good performance against unmodeled dynamics, insensitivity to parameter variations, and an excellent rejection to the external disturbances [25]. Moreover, the SMC has been used in order to control several types of induction machines in the last decade and good results has been obtained [26]-[28].

This work presents a real time SMC scheme in order to improve the power generation of a DFIG implemented in a OWC wave power plants. The proposed control scheme regulates the turbine speed in order to track the desired speed that maximize the power extraction from the Wells turbine because it optimizes the Wells turbine efficiency. This optimization of the Wells turbine efficiency is obtained selecting the flow coefficient value that maximizes the power generation. Moreover, this optimization of the Wells turbine efficiency, that maximizes the power generation, also avoids the

stalling phenomenon because the proposed control scheme maintains the flow coefficient at the best efficiency point (bep) below the stalling point. There are several works in the literature that regulates the turbine speed in order to avoid the stalling behaviour [29]-[31]. However in these works the turbine speed is not regulated in order to follow a reference speed that follows the variation of the airflow speed in order to obtain the best flow coefficient that maintains the system in the bep despite variations of the airflow speed.

The turbine speed is controlled by means of the rotor current of the DFIG using the sliding mode control theory. Regulating the turbine velocity, the proposed control scheme optimizes the flow coefficients in order to obtain the maximum power extraction in the wave power generation plant under system uncertainties and wave power variations.

In order to confirm that the designed controller meets the proposed goals. First, this controller for a DFIG used in a wave power generation plant is validated using the Matlab/Simulink software. In these simulations several operating conditions are tested and satisfactory results are obtained.

Next, the real performance of the proposed control scheme is also validated over a real experimental platform based in a DFIG. The main componentes of this control platform are the dSPACE DS1103 Controller Board, the commercial induction machine Leroy Somer of 7.5 kW and the synchronous AC servo motor 190U2 Unimotor of 10.6 kW. The stator of the DFIG is directly connected to the grid and the rotor of the DFIG is also connected to the grid through the VFC. The shaft of the DFIG and the shaft of the synchronous AC servo motor are mechanically connected so the AC servo motor emulates the torque profiles that the Wells turbine generates as response to the oscillations of the free surface in the OWC chamber. In this experimental platform several real tests, employing different operating conditions, are carried out and the obtained results are satisfying.

This paper is organized as follows: in Section 2 is presented a theoretical modelling of the OWC wave power plant that incorporates a Wells turbine. In Section 3 the design of the proposed sliding mode controller that optimizes the power generation and avoids the stalling phenomenon is presented. Section 4 presents the simulation and the experimental results developed in the experimental platform that is also described in this section. Finally, some concluding remarks are presented in Section 5.

2. Modeling of the OWC Plant

The hydrodynamic energy of the waves can be transformed to an oscillating air flow using the OWC device shown in Figure 1.

The OWC system is composed of a fixed or floating hollow structure, open to the sea below the water surface, that traps air above the inner free-surface. Wave action alternately compresses and decompresses the trapped air which is forced to flow through a turbine that generates the rotational energy [16]. This turbine is connected to a generator by means of a gear box in order to produce the electrical energy [32]. It should be noted that the airflow in the chamber is bidirectional depending if the wave is hitting or it is reflected. In this sense, to produce a continuous unidirectional rotation of the

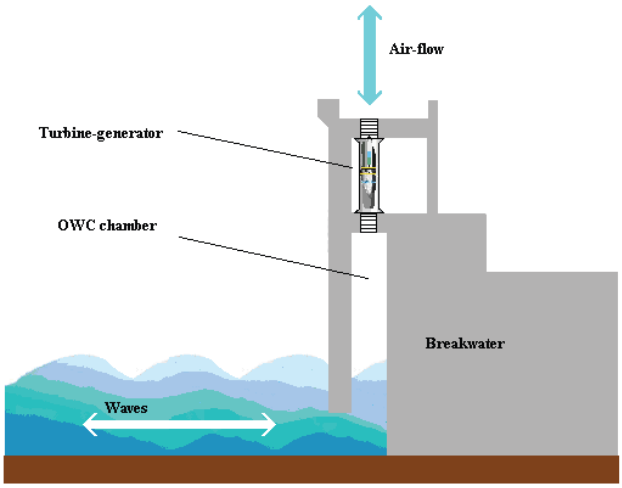

Figure 1: OWC wave power system

electrical generator, the Wells turbine can be used in order to generate the rotational energy. The Wells turbine is a low-pressure air turbine that, independent of the direction of the air flow, rotates continuously in one direction. Prof. Alan Arthur Wells of Queen's University Belfast designed this turbine in the late 1970s.

The power from the OWC available to a turbine is:

$$P_{in} = \Delta p \cdot v_x a \tag{1}$$

where v_x (m/s) is the airflow speed, Δp (Pa) is the pressure drop across the turbine, ρ (kg/m^3) is the air density and a (m^2) is the area of the section of the turbine.

In the OWC system considered in this work, the turbogenerator module is composed by a Wells turbine mechanically connected to an air-cooled DFIG by means of a gearbox in order to increase the rotational speed and accordingly to reduce the mechanical torque.

The rotor circuit of the DFIG is connected to the grid through a VFC and the active power flow between the rotor circuit and the grid must be controlled, both in magnitude and in direction, in order to produce electrical active power to the utility grid at constant frequency and voltage. Moreover, in this machine the rotor speed value can operate in an extended range from subsynchronous speed to supersynchronous rotational speed.

The VFC is composed of two four quadrant IGBT PWM converters usually called grid side converter (on the side of the grid) and rotor side converter (on the side of the rotor). These converters are back to back connected by means of a DC link capacitor.

It should be noted that in this configuration the power electronic converters only need to handle a small portion of the nominal power (around 25%-30%) in order to produce the electrical power in the grid, because only the rotor power goes to the grid

through the VFC. The stator power goes directly to the grid. Therefore, the power converters used in this configuration are smaller that the power converters used in other configurations. Therefore, the power losses and the power electronic converters cost are also smaller which is the main advantage of this configuration.

In the OWC systems, the turbogenerator may include an inertia wheel drive in order to smooth the output power curve. This inertia wheel makes the system particularly appropriate for the implementation of sliding mode control schemes because the undesired chattering, that could appear in this kind of controllers, will be mechanically absorbed by the inertia of the system.

As it has been indicated previously, a Wells turbine have been considered in this work in order to extract the mechanical energy from the airflow. The Wells turbine presents a robust and simple symmetrical blade design and therefore the Wells turbine always turns in the same direction, regardless of the direction in which the airflow passes through the turbine. The equations used for the modeling of the turbine are given by [32]:

$$\Delta p = C_a\, k\, \frac{1}{a}\left[v_x^2 + (r\, w)^2\right] \quad (2)$$

$$T_t = C_t\, k\, r\left[v_x^2 + (r\, w)^2\right] \quad (3)$$

$$T_t = \frac{C_t\, r\, a}{C_a} dP \quad (4)$$

$$k = \rho\, b\, n \frac{l}{2} \quad (5)$$

$$\phi = \frac{v_x}{rw} \quad (6)$$

$$q = v_x\, a \quad (7)$$

$$\eta = \frac{T_t\, w}{q\, \Delta p} = \frac{C_t}{C_a \cdot \phi} \quad (8)$$

where C_a is the power coefficient, C_t is the torque coefficient, the generated torque is T_t (N m), ϕ is the flow coefficient, k (kg/m) is a turbine constant, r (m) is the turbine radius, w (rad/s) is the turbine angular velocity, the blade span is b (m), the blade number is n, the blade chord is l (m), the rate of the flow is q (m^3/s), a (m^2) is the area of the section of the turbine and the efficiency of the turbine is η.

The previous equations show that the torque and the power generated by the Wells turbine can be calculated based on the torque coefficient and the power coefficient respectively. Moreover, the characteristic curves of the Wells turbine are composed by the relationship between the torque coefficient and the power coefficient versus the flow coefficient.

Due to the characteristic dynamics of the Wells turbine, when the velocity of the airflow surpasses one critical value (that is related to the Wells turbine rotational velocity), the performance of this turbine fall down drastically [32]. This effect is usually called stalling phenomenon. The Wells turbine stalls when the relative angle between the tangential speed of the turbine and the axial velocity of the input airflow is greater than a value around $14°$.

In Figure 2 can be observed the torque coefficient versus the flow coefficient ($\phi = \frac{v_x}{rw}$) for the Wells turbine used in this work. This Figure shows that the torque coefficient C_t of the Wells turbine fall down drastically when the stalling phenomenon appears. This Figure shows the characteristic curve for one particular Wells turbine and it depends on the parameters used in the turbine design. However the characteristic curves for other Wells turbines present the same behavior.

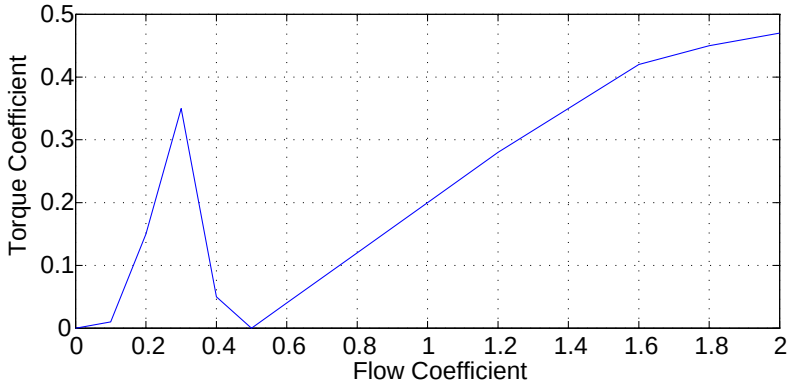

Figure 2: Torque coefficient versus Flow coefficient.

Figure 2 shows that in the Wells turbine employed in the present paper the stalling phenomenon appears when the flow coefficient reaches the value 0.3 (this value may be different depending of the the Wells turbine characteristic curve). Therefore, from this Figure it can be also concluded that for this Wells turbine a good flux coefficient value is $\phi_{bep} = 0.29$, because with this flux coefficient value the stalling behavior is avoided and the value of the torque coefficient C_t presents a local maximum.

It should be noted that, taking into account the oscillatory dynamics of the flow coefficient (due to the oscillatory movement of the air flow produced by the ocean waves) the flow coefficient value is always oscillating from zero to one positive value, so the optimum working zone for the flow coefficient is located between zero and the point of the stalling behaviour. Additionally, from eqn.(6) it is deduced that the flux coefficient could be maintained more time at its optimum value by means of the turbine velocity regulation, because when the airflow velocity increases/decreases we can increase/decrease the turbine velocity in order to maintain the flux coefficient constant in the value $\phi_{bep} = 0.29$. This turbine speed regulation, on the one hand improves the torque coefficient (and therefore improves the power generation) and on the other hand avoids the stalling behaviour.

Therefore, maximum power extraction from the ocean waves is obtained employing the next command value for the turbine velocity:

$$w^* = \frac{v_x}{r \cdot \phi_{bep}} \tag{9}$$

3. The design of the Sliding Mode Controller

In the OWC generation system that incorporates a DFIG, the objective of the maximum power extraction is achieved by regulating the rotational speed of the Wells turbine in order to avoid the stalling behaviour. In order to get this objective, a SMC scheme is proposed in order to regulate the rotor speed of the DFIG. The speed of the DFIG is regulated by means of the quadrature component of the rotor current.

In the model description it is explained that, the shaft speed of the OWC turbogenerator should be adjusted so that the flow coefficient ϕ remains bounded in order to extract the maximum power from the sea. In this case the maximum stalling free torque coefficient C_t can be obtained.

It should be noted that there is a unique generator speed reference value to satisfy the condition of optimum flow coefficient value to get the maximum wave energy extraction for a given pressure drop input dP. This value can be calculated based on the characteristic curve of the Wells turbine under consideration provided by the manufacturer. However, considering that all Wells turbines present a similar stalling behavior, this operation may always be extended to other Wells turbines.

In this sense, the control objective is similar to that used in other well established DFIG applications like wind turbines in which the maximum power point tracking control strategies are defined. In these systems, a tracking reference for the turbine speed should be followed by the control system. In this case, the reference depends on the maximum power variation with the rotational speed of the DFIG. This reference is also different for each wind turbine depending of its aerodynamic design that provides different power coefficient versus tip speed ratio characteristic curve [33].

The design of the SMC uses the knowledge of the turbogenerator dynamics, so the turbogenerator dynamics should be calculated. The turbogenerator dynamics incorporate one mechanical part and other electrical part.

The next equation represents the mechanical part for the dynamic of the turbogenerator:

$$J\dot{w} + Bw = T_t - \gamma T_e \tag{10}$$

where T_t is the torque generated in the turbine by the air flow produced by the waves, B is the viscous friction coefficient, T_e is the the generator torque, J is the inertia moment, w is the angular velocity of the turbine shaft and the gear ratio $\gamma = w_e/w$ is the relation between the angular velocity of the turbine shaft w and the angular velocity of the generator rotor w_e.

As it is well known, the field oriented control (referring all expressions to the stator flux reference frame) can be used in order to simplify the electrical equations of the DFIG. In the reference frame oriented in the stator flux, the d-axis is aligned with the stator flux linkage vector ψ_s, and then, ψ_{ds}=ψ_s and ψ_{qs}=0. Then, the next relationships are obtained [34]:

$$i_{qs} = -\frac{L_m i_{qr}}{L_s} \tag{11}$$

$$i_{ds} = \frac{L_m(i_{ms} - i_{dr})}{L_s} \tag{12}$$

$$i_{ms} = \frac{v_{qs} - r_s i_{qs}}{w_s L_m} \tag{13}$$

$$T_e = -\frac{3p}{4}\frac{L_m^2 i_{ms} i_{qr}}{L_s} \tag{14}$$

$$Q_s = \frac{3}{2}\frac{w_s L_m^2 i_{ms}(i_{ms} - i_{dr})}{L_s} \tag{15}$$

$$v_{dr} = r_r i_{dr} + \sigma L_r \frac{di_{qr}}{dt} - s w_s \sigma L_r i_{qr} \tag{16}$$

$$v_{qr} = r_r i_{qr} + \sigma L_r \frac{di_{qr}}{dt} \tag{17}$$

$$+ s w_s \left(\sigma L_r i_{dr} + \frac{L_m^2 i_{ms}}{L_s}\right) \tag{18}$$

where L_s is the stator inductance, L_r is the rotor inductance and L_m is the mutual inductance; r_r is the rotor resistance, r_s is the stator resistance, w_s is the synchronous speed; w_e is the rotor speed of the generator; the slip frequency is $sw_s = w_s - w_e$; p is the pole numbers and $\sigma = 1 - \frac{L_m^2}{L_s L_r}$.

It should be noted that the stator magnetizing current (i_{ms}) can be considered constant because the influence of the stator resistance is small and the stator is connected to the grid [21]. Accordingly, the electromagnetic torque can be calculated as follows:

$$T_e = -K_T i_{qr} \tag{19}$$

where the torque constant value K_T is calculated below:

$$K_T = \frac{3p}{4}\frac{L_m^2 i_{ms}}{L_s} \tag{20}$$

Substituting equation (19) in equation (10) the next dynamic equation may be obtained, where the uncertainty terms has also been included:

$$\dot{w} = -(c_1 + \triangle c_1)w + (f + \triangle f) - (c_2 + \triangle c_2) i_{qs} \tag{21}$$

where $c_1 = \frac{B}{J}$, $c_2 = \frac{\gamma K_T}{J}$, $f = \frac{T_t}{J}$ and the terms $\triangle c_1$, $\triangle c_2$ and $\triangle f$ represent the uncertainties of the terms c_1, c_2 and f respectively.

Then, the dynamic equation (21) can be rewritten as:

$$\dot{w} = -c_1 w + f + -c_2 i_{qs} + \Delta(t) \tag{22}$$

where the uncertainty terms have been collected in the term Δ:

$$\Delta(t) = -\triangle c_1\, w(t) + \triangle f(t) - \triangle c_2\, i_{qr}(t) \tag{23}$$

Now, in order to compensate for the above described uncertainties a sliding mode control scheme is proposed.

The speed tracking error is defined as follows:

$$e(t) = w(t) - w^*(t) \tag{24}$$

where w^* is the command for the turbine speed in order to extract the maximum power from the waves.

The previous equation can be derived with respect to time:

$$\dot{e}(t) = \dot{w} - \dot{w}^* = -c_1 w(t) + f(t) - c_2 i_{qr}(t) - \dot{w}^*(t) + \Delta(t) \tag{25}$$

Next, a SMC scheme is proposed in order to track the turbine speed command (that provides the maximum wave power extraction) despite of the system uncertainties.

The sliding variable $S(t)$ is defined as:

$$S(t) = e(t) + \int_0^t k\, e(\tau)\, d\tau \tag{26}$$

where k is a positive constant gain.

Next, the proposed sliding surface is:

$$S(t) = e(t) + \int_0^t k\, e(\tau)\, d\tau = 0 \tag{27}$$

Finally, the speed controller based on the sliding mode is obtained:

$$i_{qr}^*(t) = \frac{1}{c_2}\left[k\, e + \beta\, \mathrm{sgn}(S) - c_1\, w - \dot{w}^* + f\right] \tag{28}$$

where β is the switching gain and $\mathrm{sgn}(\cdot)$ is the sign function.

In order to achieve the tracking of the reference velocity, the next condition should be fulfilled:

($\mathcal{C}\,1$) The sliding gain β of the controller must be selected greater than the system uncertainties; that is, $\beta > |\Delta(t)|$ for all time.

The closed loop stability of the proposed control scheme (based on the control law presented in equation (28)) for the wave power plant that moves a DFIG (whose dynamic is given in equation (21)) can be proved using the Lyapunov stability theory.

Proof : The Lyapunov function candidate is defined as:

$$V(t) = \frac{1}{2} S(t) S(t) \tag{29}$$

The time derivative of the previous Lyapunov function candidate is:

$$\begin{aligned}
\dot{V}(t) \;=\;& S(t)\dot{S}(t) \\
=\;& S \cdot [\dot{e} + ke] \\
=\;& S \cdot [-c_1 w + f - c_2 i_{qr} - \dot{w}^* + \Delta + k\, e] \\
=\;& S \cdot [-c_1 w + f - (k\, e + \beta\, \mathrm{sgn}(S) - c_1\, w - \dot{w}^* + f) - \dot{w}^* + \Delta + k\, e] \\
=\;& S \cdot [\Delta - \beta\, \mathrm{sgn}(S)] && (30) \\
=\;& \Delta\, S - \beta |S| && (31) \\
\leq\;& |\Delta||S| - \beta |S| \\
\leq\;& 0 && (32) \\
& && (33)
\end{aligned}$$

It should be indicated that the eqns. (26), (25) and (28) and the condition $(\mathcal{C}\,1)$ have been employed in this proof.

Taking into account that $V(t)$ is clearly positive-definite, $\dot{V}(t)$ is negative definite and $V(t)$ tends to infinity as $S(t)$ tends to infinity, the Lyapunov's direct method can be used to conclude that the equilibrium at the origin $S(t) = 0$ is globally asymptotically stable. Therefore $S(t)$ tends to zero as the time tends to infinity. Further, the trajectories starting off the sliding surface $S = 0$ must reach the sliding surface in finite time and then will remain on it. The behavior of this system on the sliding surface is habitually called *sliding mode* [25].

It should be noted that when the system reaches the sliding surface Eqn.(27), then $S(t) = \dot{S}(t) = 0$, and accordingly the tracking problem of this system presents an equivalently dynamic behavior given by the following equation:

$$\dot{S}(t) = 0 \quad \Rightarrow \quad \dot{e}(t) = -(k + a)e(t) \tag{34}$$

Then, taking into account that $k > 0$, it is clear that the tracking error $e(t)$ converges to zero exponentially.

It should be pointed out that the habitual motion in the sliding mode control consists of two phases. First, *reaching phase* when the trajectories starting off the sliding surface $S = 0$ move toward it and reach it in finite time. Second *sliding phase* when the system motion is confined to the sliding surface and then the system tracking error is equivalently represented by the reduced-order model (eqn.34). In this phase, the tracking error tends to zero as the time tends to infinity.

Accordingly, the turbine speed of this wave power generation plant can be regulated using he proposed sliding mode control in order to obtain the maximum ocean wave power extraction by means of the Wells turbine considering that there are unmodelled dynamics and system uncertainties. This is because the turbine speed tracks the reference speed value to obtain the optimum flow coefficient in order to maximise the power extraction from the Wells turbine.

4. Experimental Results

The behaviour for sliding mode controller proposed in this paper is analysed in this section.

Figure 3 shows the block diagram for the experimental platform that we have employed to develop the real time experimental validation, and in Figure 4 it can be observed a photography for this platform.

The experimental platform has been designed and constructed using industrial components. The main componentes of this experimental platform are the Real Time Controller Board of dSPACE model DS1103 that is based on a floating point PowerPC processor to 1 GHz. The DFIG is an industrial electric machine of 7.5 kW, 1447 rpm developed by Leroy Somer whose paremeter are indicated in Table 1. The stator of this DFIG is connected to the grid and the rotor is also connected to the grid but by

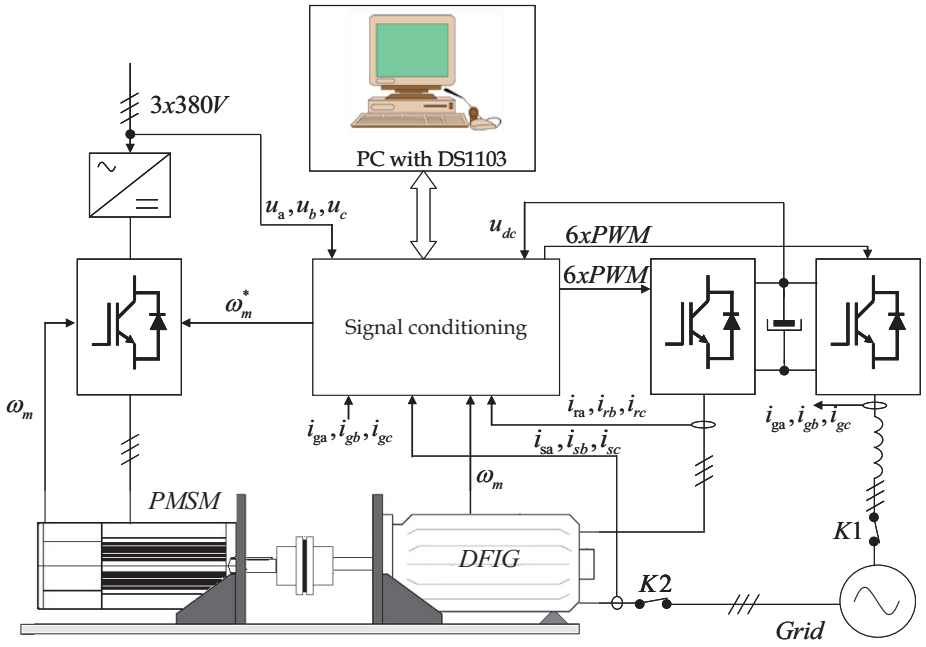

Figure 3: Block diagram of the experimental platform

means of two voltage source inverters, developed by MONTELEC S.L., model NFS-200-10 that are placed in a Back to Back configuration. The proposed control schemes are programed using a PC with the software MatLab7/Simulink R2007a and dsControl 3.2.1.

In this experimental platform, the mechanical torque profiles, produced by the Wells turbine, are calculated using a Wells turbine model implemented in Simulink. The parameters of the Wells turbine employed in the Simulink model are presented in Table 2. The dynamic of the Wells turbine can be obtained using the characteristic curves of the turbine under study ([32], [35]). Accordingly, the torque, the power and the efficiency produced by the wells turbine can be calculated based on the torque coefficient against the flow coefficient (Figure 2), the power coefficient against the flow coefficient (Figure 5) and the efficiency against the flow coefficient (Figure 6).

The mechanical torque profiles are obtained from the Simulink model of the Wells turbine and then generated in the real platform using a synchronous AC servo motor of 10.6 kW model 190U2 of Unimotor. The shaft of this AC servo motor is mechanically coupled to the shaft of the DFIG in order to move the rotor of the DFIG. The servo

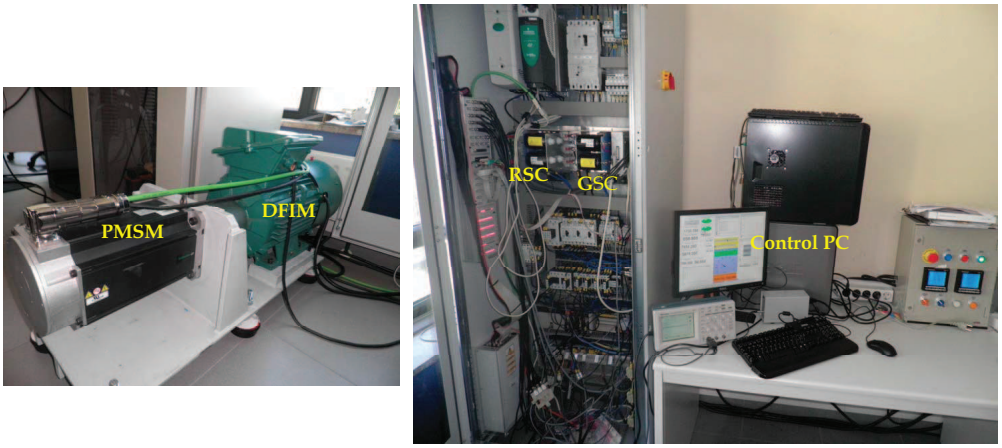

Figure 4: Photography of the experimental platform

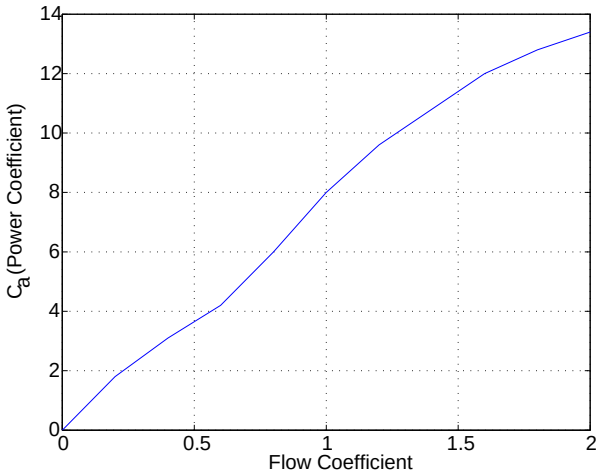

Figure 5: Power coefficient versus flow coefficient.

motor incremental encoder of 4096 square impulses per revolution are employed in order to measure the rotor velocity using the frequency measurement method.

In order to protect the machine against over currents, the stator and the rotor currents are limited to their nominal values. All the sensors to measure the voltages, speed and currents are adequately adapted in order to be connected to the DS1103 Real Time Controller Board.

The DS1103 Controller Board controls both inverters generating the SVPWM (space

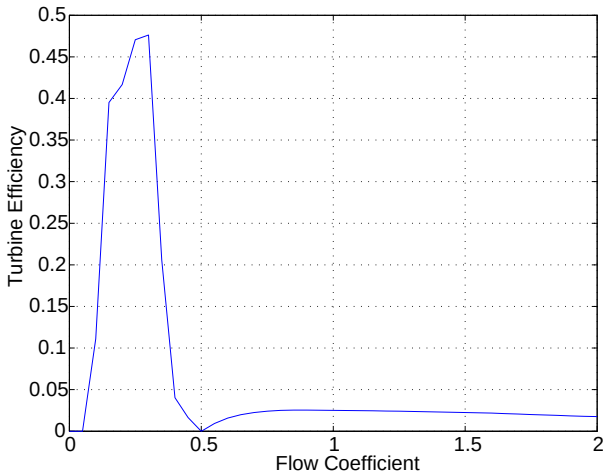

Figure 6: Efficiency versus flow coefficient

Stator Voltage	380 V
Rotor Voltage	190 V
Rated stator current	18 A
Rated rotor current	24 A
Rated speed	1447 r.p.m.@ 50 Hz
Rated torque	50 Nm
Stator resistance	0.325 Ω
Rotor resistance	0.275 Ω
Magnetizing inductance	0.0664 H
Stator leakage inductance	0.00264 H
Rotor leakage inductance	0.00372 H
Inertia moment	0.07 kg.m^2

Table 1: Ratings and parameters of the DFIG (Leroy Somer).

n	=	8
l	=	0.38 m
a	=	1.1763 m^2
b	=	0.4 m
k	=	0.7079
r	=	0.7285 m
Gear ratio	=	5

Table 2: Wells turbine parameters.

vector pulse width modulation) pulses. The sample period is defined for the SVPWM frequency of 7 kHz, this is 143 μs. The dead time for the inverters used in this study is 1.5 μs and is controlled by software and hardware. The connection sequence of the DFIG to the grid begins with the charging of rotor and grid converters DC bus. Once this DC bus is charged and if the grid side reference system is oriented with the grid voltage, then the grid side converter is connected through contactor K1 and the regulation of DC bus to a fixed value begins.

The next two steps have to be taken into account before connecting the stator of the DFIG to the grid. The first step is the encoder offset detection with respect to the stator flux. The second step is the stator voltage synchronization with respect to the grid voltage. The synchronization of the DFIG stator voltage with the grid voltage is realized by measuring the grid side voltage and using a PLL (Phase Locked Loop). Then, after the realization of these two steps the stator of the DFIG can be connected to the grid using the contactor K2 and then the reactive and active power regulation can begin.

4.1. Simulations and real platform validation

In order to avoid undesirable damages in the experimental platform, one simulation model for the experimental platform has been designed and implemented in Matlab/Simulink to test the controllers in advance. In this sense, the new controllers are tested and tuned in advance using the simulation model and then these controllers are implemented and adjusted in the experimental platform in order to show their real performance.

In order to show that the real system and the simulation model implemented in Matlab/Simulink are very close, the next experimental validation using the Matlab/Simulink and the real experimental platform has been carried out.

In this experimental validation, the DFIG speed is maintained constant at 1432 rpm with a reactive power of 0 VAR. It is supposed a scenario where the waves produce a typical variation in the pressure drop given by $dP = |1800 \cdot \sin(0.3t)|$ as shown in Figure 7 during 25 seconds. The turbine flow coefficient obtained in this experimental validation are shown in Figure 8 for the simulation case and in Figure 9 for the real platform. As it can be observed these figures are very similar, so this validates the good performance of the model for the OWC system that we have designed and implemented in the MATLAB/Simulink software.

It should be noted that for this pressure drop condition the turbine flow coefficient ϕ exceeds the limit value of 0.30, so the undesirable stalling behaviour will appear in the Wells turbine system. In this sense, Figure 10 for the simulation case and Figure 11 for the real platform, show a significant reduction in the torque coefficient due to the turbine stalling behaviour. This reduction in the torque coefficient, due to the turbine stalling behaviour, induces a strong reduction in the output power obtained in the DFIG, as it can be observed in Figure 12 for the simulation case and in Figure 13 for the real platform. These figures show the rotor power, the stator power and the total power obtained in the DFIG, that is the sum of the the rotor power and the stator power. It should be noted that the power value is negative because the electric machine is generating power. Finally, Figure 14 shows the efficiency of the Wells turbine under the flow

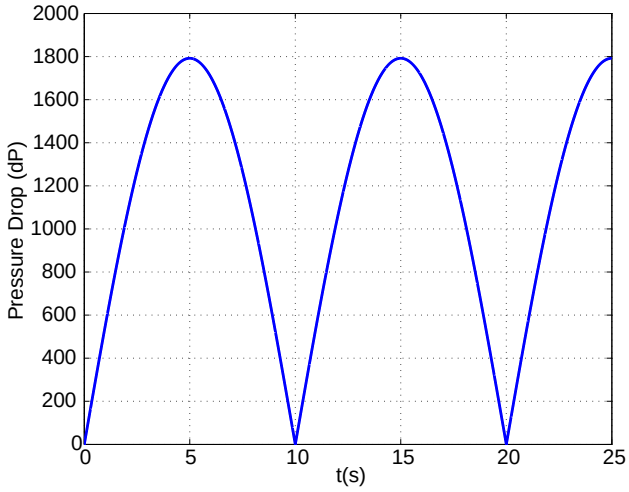

Figure 7: Pressure drop dP used as input for the emulated Wells turbine in the simulation and in the real platform

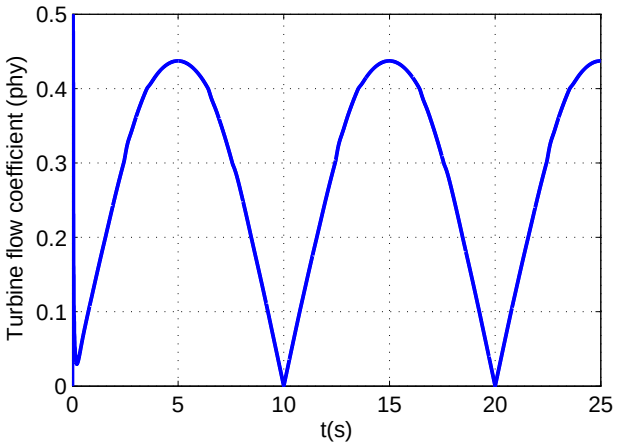

Figure 8: Turbine flow coefficient for the simulation under constant turbine speed

coefficient show in Figure 9. This efficiency value is obtained using the characteristic curve of the Wells turbine efficiency presented in Figure 6.

In order to avoid the problem of the turbine stalling behaviour caused by the high value of the flow coefficient that exceeds the limit value of 0.30, the rotor speed of the DFIG can be regulated in order to maintain the flux coefficient below the limit value of 0.30 as it is shown in the next subsection. Moreover, in order to improve the power generated by the Wells turbine the rotor speed can also be regulated in order to follow

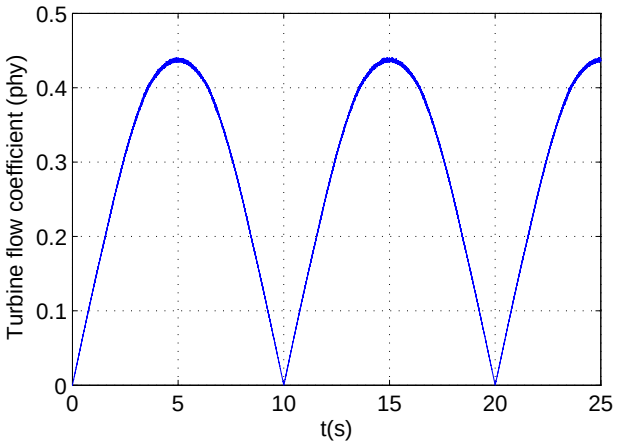

Figure 9: Turbine flow coefficient for the real platform under constant turbine speed

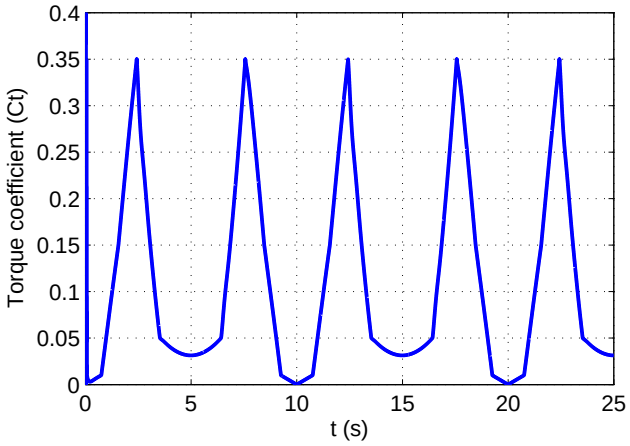

Figure 10: Turbine torque coefficient for the simulation under constant turbine speed

the reference value provided by eqn.(9) that optimizes the flow coefficient value and accordingly improves the torque value and therefore increments the power generated.

Finally it can be observed that the results obtained in the simulation case and in the real platform are very similar, showing that the simulation model approximates accurately the real platform. Therefore, these results demonstrates that the simulation model will be very useful in order to adjust in advance the controllers that will be implemented in the real platform.

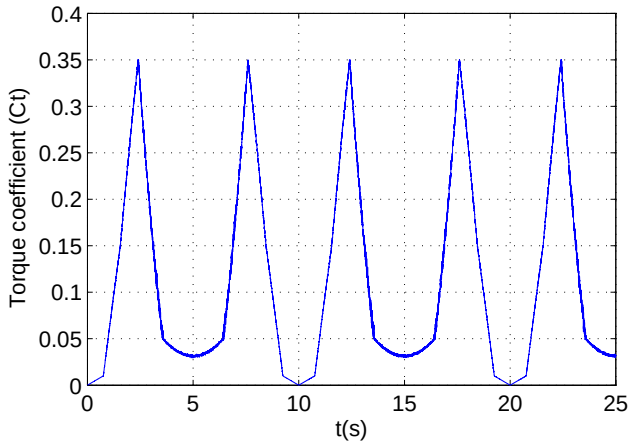

Figure 11: Turbine torque coefficient for the real platform under constant turbine speed

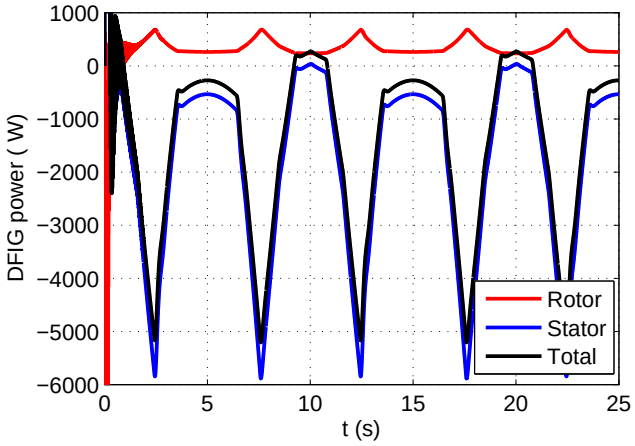

Figure 12: DFIG generated power for the simulation under constant turbine speed

4.2. DFIG speed control

In this section the speed regulation performance for the turbo generator using the proposed sliding mode field oriented control scheme under model uncertainties is tested in the real platform. The case of study considers a scenario where the waves produce a typical variation in the pressure drop given by $dP = |1800 \cdot \sin(0.3t)|$ as it is shown in Figure 7. In this case the rotor speed of the DFIG is controlled in order to follow the speed reference given by equation (9) so as to maintain the flux coefficient at its optimum value ($\phi_{bep} = 0.29$) in order to maximizes the torque value and below the limit value of $\phi = 0.30$ in order to avoid the stalling. In this test the imposed reactive power in the DFIG control is 0 VAR. According to the emulated Wells turbine parameters and

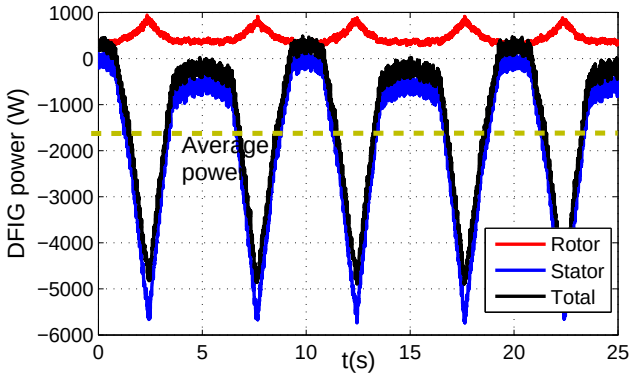

Figure 13: DFIG generated power for the real platform under constant turbine speed

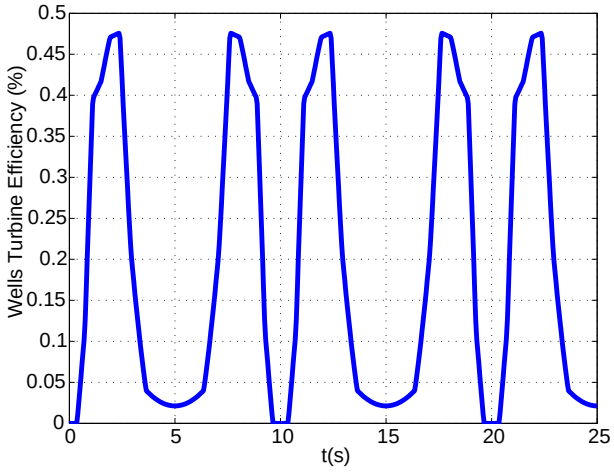

Figure 14: Efficiency of the Wells turbine under constant turbine speed

with the given pressure drop, the speed reference for the DFIG to get the maximum power is shown in Figure 15. This Figure also shows the real speed obtained using the proposed sliding controller in the real platform. In Figure 15 it can be observed that the proposed controller provides a good behaviour because a good speed tracking is obtained under system uncertainties. The values for the speed sliding controller are, $\beta = 40$, $k = 31$. These parameters are experimentally tuned, taking into account the influence of these parameters in the controller performance. The β parameter should be selected bigger than the system uncertainties, but it should be noted that when ß increases the control effort also increases which is undesirable. An increase in parameter k gives an increase in the position error convergence when the system reaches the sliding surface $S(t) = 0$, but this also increases the control effort which is undesirable.

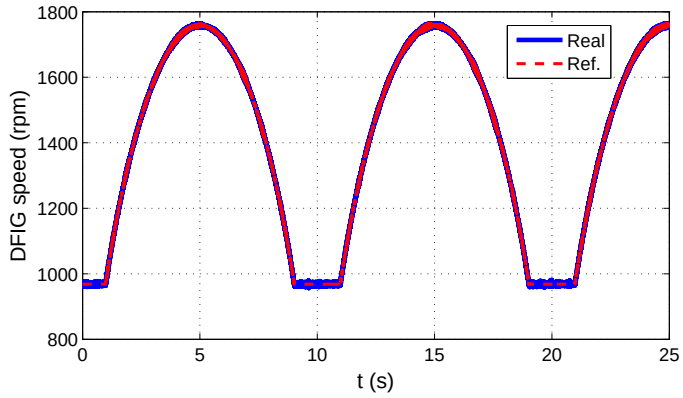

Figure 15: DFIG real and speed reference for a $dP = |1800\sin(0.3t)|$ using the proposed SMC.

In this experimental validation the same pressure drop variation given by $dP = |1800 \cdot \sin(0.3t)|$ that was employed in the previous test is used. However, in this test the proposed sliding mode controller is employed in order to regulate the rotor speed of the DFIG. The flow coefficient obtained in this case is shown in Figure 16.

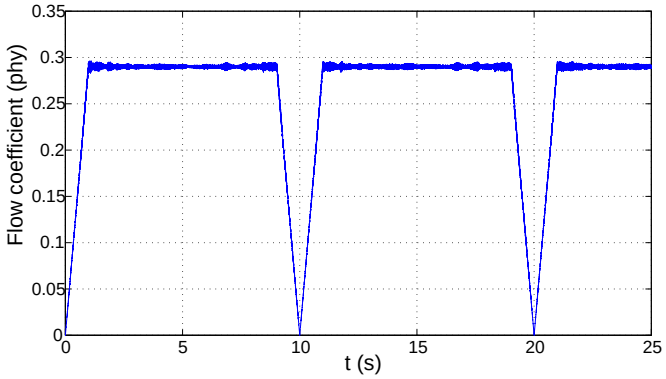

Figure 16: Flow coefficient using the proposed SMC

In this Figure it can be observed that the flow coefficient is maintained most of the time at its optimum value ($\phi_{bep} = 0.29$) in order to maximizes the torque value and also below the limit value of 0.30 in order to avoid the turbine stalling behaviour. Moreover, in this case, the turbine speed regulation allows to maintain the torque coefficient at its maximum value below the stalling point over a wide range of time, as it is shown in Figure 17, so in this case the maximum wave power generation is obtained.

Figure 18 shows the efficiency of the Wells turbine under the flow coefficient show in Figure 16. Comparing figures 14 and 18 it is observed that the efficiency of the Wells turbine is greatly improved using the proposed sliding mode control for the tracking of

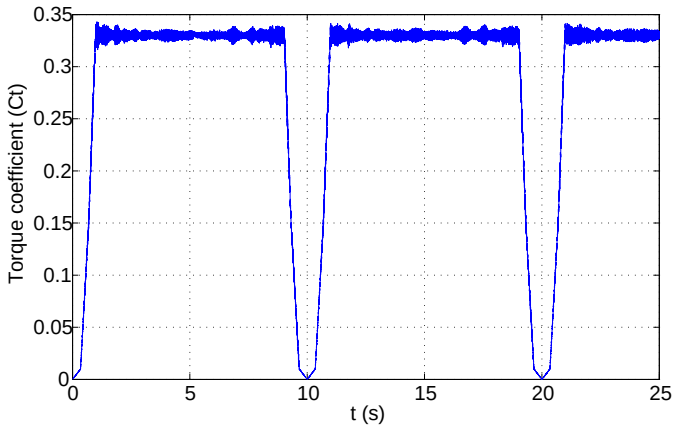

Figure 17: Torque coefficient using the proposed SMC

the optimum turbine reference speed, because in this case the optimum value for the flow coefficient, and therefore the optimum value for the torque coefficient, is maintained during most of the time.

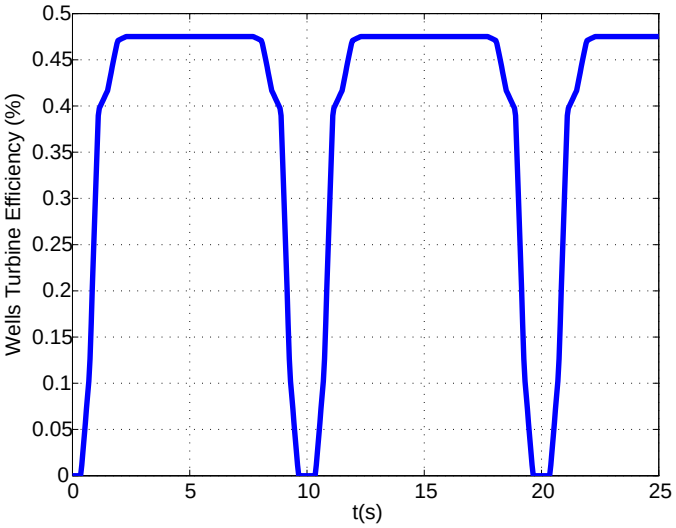

Figure 18: Efficiency of the Wells turbine using the proposed SMC

Figure 19 shows the power generated in the DFIG. This Figure shows the rotor power, the stator power and the total power obtained in the DFIG. In this Figure it can be observed that the rotor power is changing the polarity according to the DFIG speed. When the speed is higher than the synchronous speed, the value is negative indicating

that energy is obtained from the waves and returned to the grid. So, in that moment the total power is higher than the stator power. On the other hand, when the machine performs below the synchronous speed the stator power is higher than the total power because the rotor is getting energy from the grid. The obtained total average power is 5000 W with peaks of 8000 W.

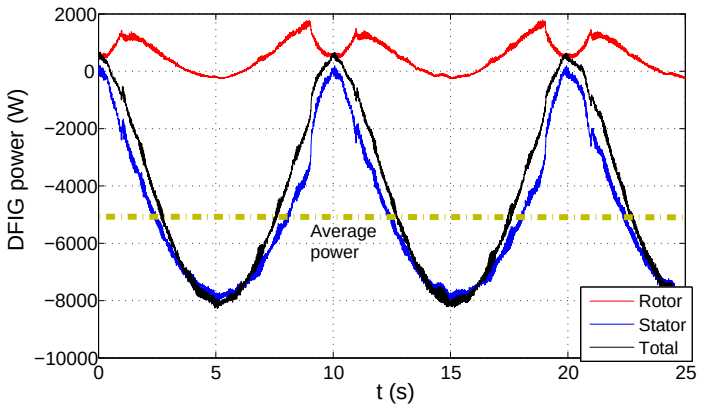

Figure 19: DFIG generated power using the proposed SMC

Figures 20 and 21 shows the rotor and stator currents respectively. As it can be observed in these figures, the quality of the current injected into the grid is quite good. It should be noted that although there are large variations in the power, due to the variations in the pressure drop, these variations are dynamically slow compared with the current control dynamic of the DFIG. Therefore, despite having great variations in power and speed that produce large variations in the current, the quality of the wave in the current injected into the grid is good at all times.

Figure 22 shows the rotor, stator and total power for two different reactive power references, 0 VAR and 5 kVAR that changes at time t=14.5s as it is shown in Figure 23. As it can be observed, in the transition between both reactive powers, the active power has a fast transition due to the controlled speed, so a good behaviour between reactive power variations is obtained using this sliding mode controller. It should be noted that when a DFIG is controlled, active and reactive powers are regulated. It is important to show that variations in the active power are independent from the reactive power and vice versa. Figures 22 and 23 show that despite the variations of the active power (P) and the reactive power (Q) both are correctly regulated without interfering with each other.

Figure 24 and Figure 25 show the speed regulation performance, for a PI controller and the proposed sliding mode controller respectively, if a sudden change in the pressure drop goes from $dP = |1800 \cdot \sin(0.3t)|$ to $dP = |1520 \cdot \sin(0.3t)|$ when the DFIG speed is at its maximum value.

The sliding mode controller response, shown in Figure 25, gives a better behaviour compared with the PI controller response shown in Figure 24 because the SMC con-

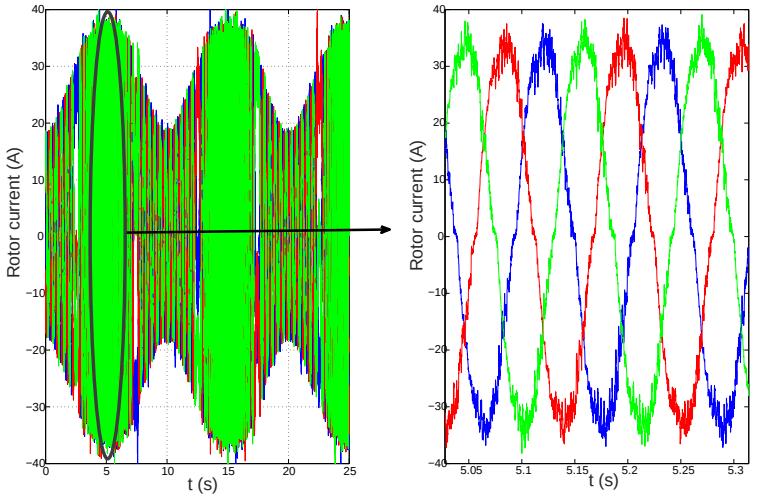

Figure 20: DFIG rotor currents using the proposed SMC

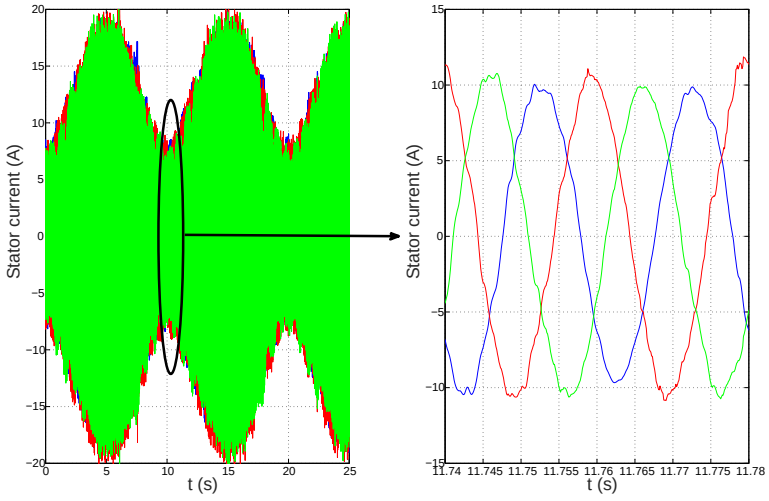

Figure 21: DFIG stator currents using the proposed SMC

troller presents a better reference tracking. Obviously, the overshoot presented in the the PI control case can be reduced but at the cost of a slower response.

Next, the ability of the method to control a real power plant is tested using JONSWAP (Joint North Sea Wave Project) spectra ([37]) that defines the distribution of

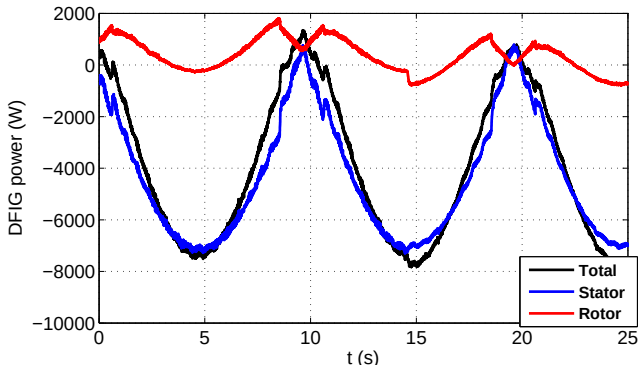

Figure 22: DFIG generated power in a reactive power step using the proposed SMC

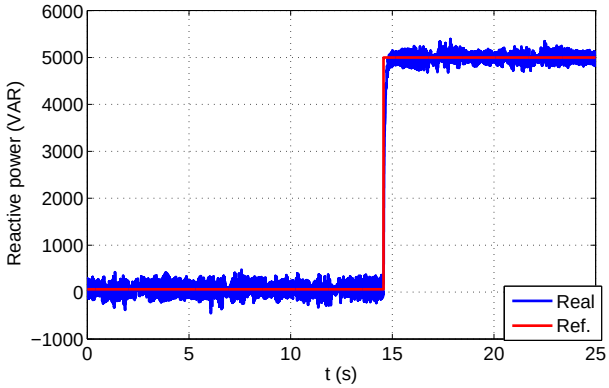

Figure 23: Reactive power step using the proposed SMC

wave energy density among different wave frequencies on the North Sea. This spectra is shown in Figure 26.

Figure 27 shows the mechanical torque produced for the Wells turbine under presume drop of Figure 26 and the torque in the DFIG, that is reduced due to the gear ratio between the turbine and the DFIG.

Figure 28 shows the reference and the real DFIG speed that is obtained using the proposed SMC control in order to improve the flow coefficient and also in order to avoid the stalling.

The flow coefficient for this spectra is presented in Figure 29. In this figure it can be observed that the flow coefficient is maintained at the optimum value of $\phi_{bep} = 0.29$ a lot of the time and also that the stalling is avoided.

Figure 30 shows the Wells turbine efficiency and, as it can be observed, thanks to the flow coefficient optimization the Wells turbine efficiency is improved because the efficiency value is maintained in the maximum point during more time.

Finally, Figure 31 shows the power generated in the DFIG. This figure shows the

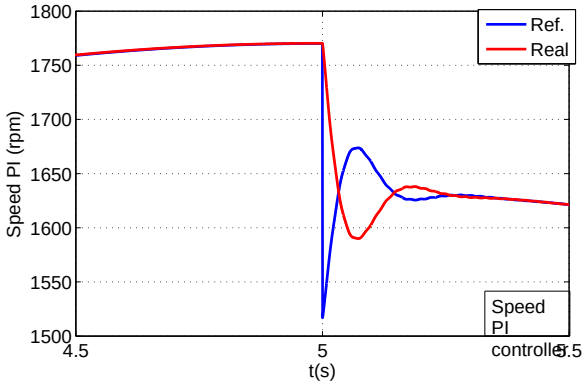

Figure 24: Speed regulation in a PI controller after a sudden change in the pressure drop.

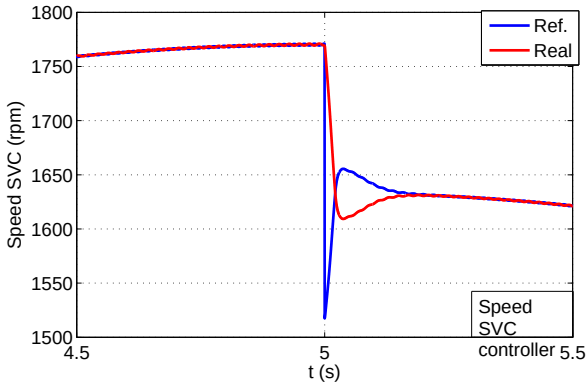

Figure 25: Speed regulation in the proposed SMC controller after a sudden change in the pressure drop.

rotor power, the stator power, the total power, and the average power.

5. Conclusions

This paper proposes a SMC scheme for wave power generation plants. As it is well known, the sliding mode control is robust under uncertainties caused by system disturbances and modelling errors. The proposed control method maximizes the power extraction for wave power plants using a Wells turbine because the controller regulates the Wells turbine velocity in order to operate in the maximum power efficiency. In this sense, the control of the turbine velocity provides an optimum flow coefficient value for the Wells turbine that produces an optimum torque coefficient and accordingly the maximum wave energy extraction is obtained.

On the other hand, this speed regulation is also used to avoid the stalling behaviour in the Wells turbine dynamics, because the flow coefficient can be maintained below

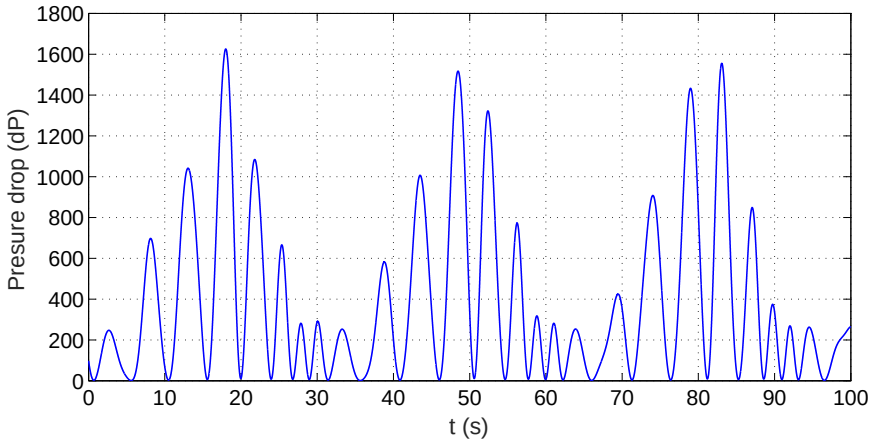

Figure 26: Pressure drop obtained according to the JONSWAP spectra.

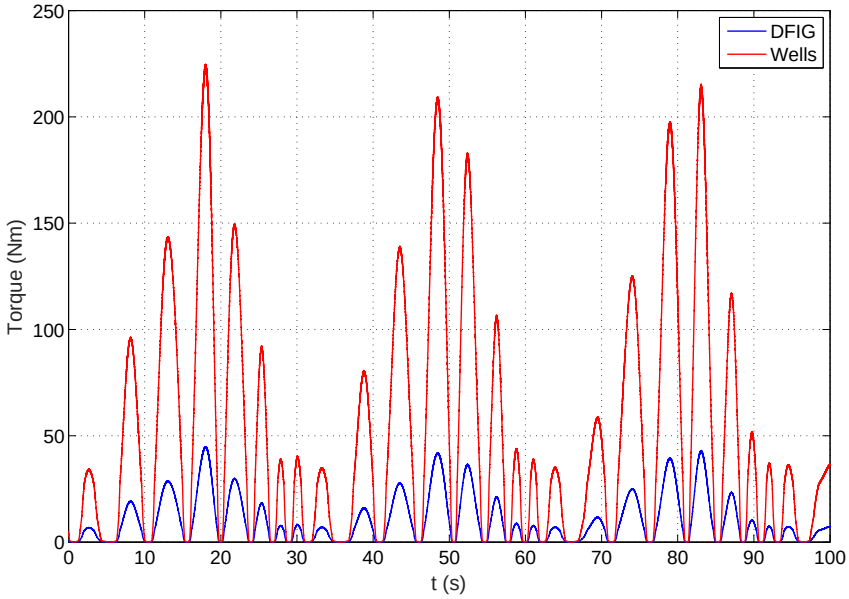

Figure 27: Torque produced for the Wells turbine and DFIG torque for the given JONSWAP spectra.

the critical value.

In this work, the Lyapunov stability theory is employed in order to demonstrate the closed-loop stability of the proposed design. Then, this control scheme has been successfully validated by means of some simulation examples. The simulation re-

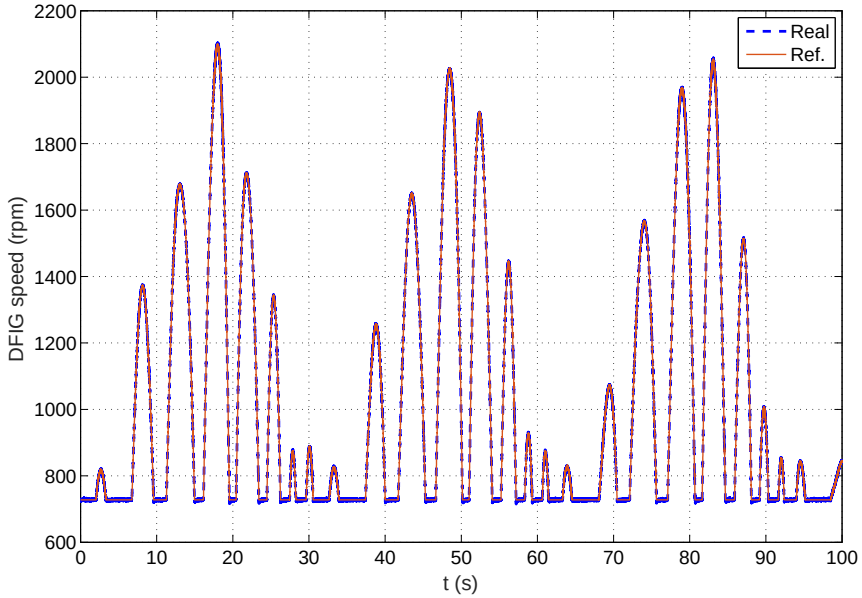

Figure 28: Reference and real DFIG speed for the given JONSWAP spectra.

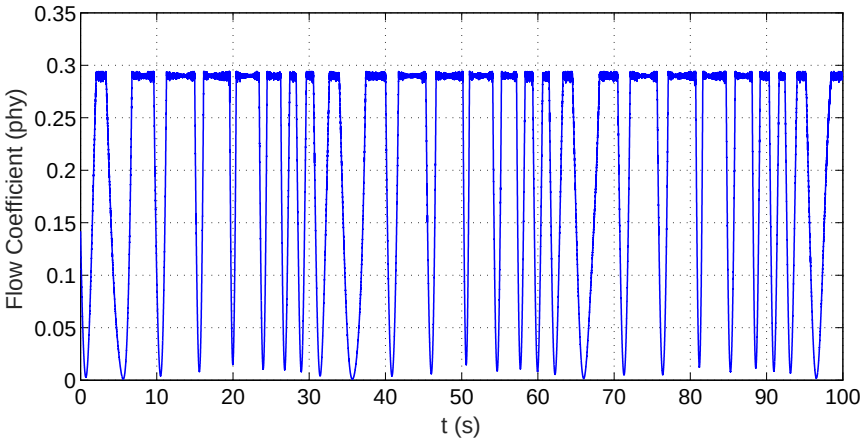

Figure 29: Flow coefficient for the given JONSWAP spectra.

sults show that the proposed SMC strategy presents a good regulation of the turbine speed and thanks to this control scheme the optimum value for the flow coefficient is achieved. As a result of this optimum value for the flow coefficient, the Wells turbine can extract the maximum mechanical power from the waves and therefore the maxi-

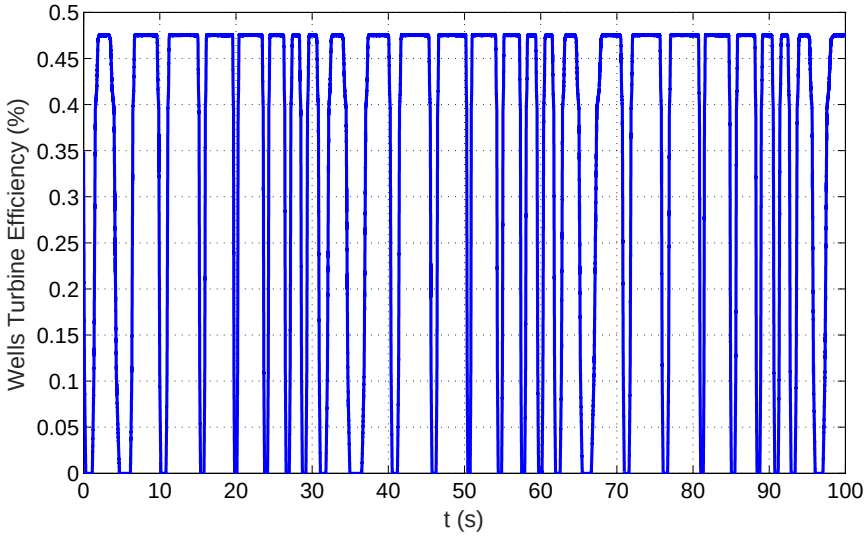

Figure 30: Efficiency for the given JONSWAP spectra.

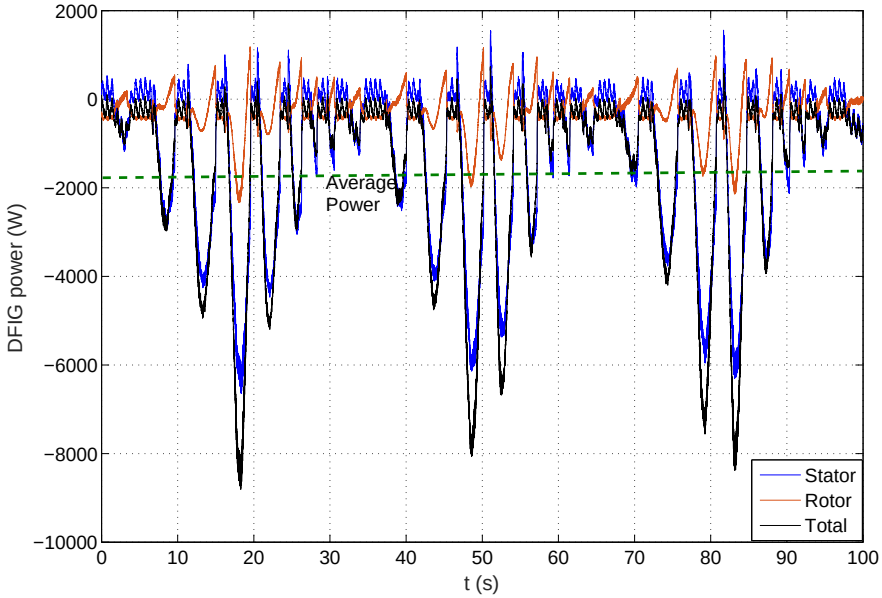

Figure 31: DFIG Stator, rotor, total and average power for the given JONSWAP spectra.

mum electrical power can be also generated.

Finally, some real tests in a new control platform that has been designed and constructed have been carried out. These tests have been shown that the proposed control

scheme presents a good performance in the real system, because a good tracking for the reference velocity is obtained under system uncertainties. Then the proposed real time SMC improves the Wells turbine efficiency in an OWC system.

Acknowledgments

The authors are very grateful to the UPV/EHU by its support through the projects PPGA18/04 and UFI11/07 and to the Basque Government by its support through the project ELKARTEK 2017. The authors also would like to thank the anonymous reviewers who have helped to improve the initial version of this paper.

References

[1] M. Lopez, M. Veigas, G. Iglesias, On the wave energy resource of Peru, *Energy Conversion and Management*, vol. 90, pp. 34-40. 2015.

[2] B.G. Reguero, I.J. Losada, F.J. Méndez, A global wave power resource and its seasonal, interannual and long-term variability, *Applied Energy*, vol. 148, pp. 366-380. 2015.

[3] Helen Bailey, Bryson R.D. Robertson, Bradley J.Buckham, Wave-to-wire simulation of a floating oscillating water column wave energy converter, *Ocean Engineering*, vol. 125, pp. 248-260. 2016.

[4] Fernando R.Torres, Paulo R.F.Teixeira, Eric Didier, Study of the turbine power output of an oscillating water column device by using a hydrodynamic – Aerodynamic coupled model, *Ocean Engineering*, vol. 125, pp. 147-154. 2016.

[5] De-Zhi Ning, Rong-Quan Wanga, Qing-Ping Zou, Bin Teng, An experimental investigation of hydrodynamics of a fixed OWC Wave Energy Converter, *Applied Energy*, vol. 168, pp. 636-648. 2016.

[6] Daewoong Son, Ronald W. Yeung, Optimizing ocean-wave energy extraction of a dual coaxial-cylinder WEC using nonlinear model predictive control, *Applied Energy*, vol. 187, pp. 746-757. 2017.

[7] N.M. Tom, Y.H. Yu, A.D. Wright, M.J. Lawson, Pseudo-spectral control of a novel oscillating surge wave energy converter in regular waves for power optimization including load reduction, *Ocean Engineering*, vol. 137, pp. 352-366. 2017.

[8] Farrokh Mahnamfar, Abdüsselam Altunkaynak, Comparison of numerical and experimental analyses for optimizing the geometry of OWC systems, *Ocean Engineering*, vol. 130, pp. 10-24. 2017.

[9] K. Rezanejad, C. Guedes Soares, I. Lopez, R. Carballo, Experimental and numerical investigation of the hydrodynamic performance of an oscillating water column wave energy converter, *Renewable Energy*, vol. 106, pp. 1-16. 2017.

[10] António F.O. Falcão, João C.C. Henriques, Oscillating-water-column wave energy converters and air turbines: A review, *Renewable Energy*, vol. 85, pp. 1391-1424. 2016.

[11] Paresh Halder, Abdus Samad, Dominique Théevenin, Improved design of a Wells turbine for higher operating range, *Renewable Energy*, vol. 106, pp. 122-134. 2016.

[12] Ahmed S. Shehata, Qing Xiao, Khalid M. Saqr, Ahmed Naguib, Day Alexander, Passive flow control for aerodynamic performance enhancement of airfoil with its application in Wells turbine – Under oscillating flow condition, *Ocean Engineering*, vol. 136, pp. 31-53. 2017.

[13] R. Carballo, G. Iglesias, "A methodology to determine the power performance of wave energy converters at a particular coastal location", *Energy Conversion and Management*, vol. 61, pp. 8-18, 2012.

[14] I. López, B. Pereiras, F. Castro, G. Iglesias, Holistic performance analysis and turbine-induced damping for an OWC wave energy converter, *Renewable Energy*, vol. 85, pp. 1155-1163. 2016.

[15] J.C.C. Henriques, L.M.C. Gato, A.F.O. Falcão, E. Robles, F.-X. Faÿ, Latching control of a floating oscillating-water-column wave energy converter, Renewable Energy, 90, 2016, Pages 229-241, https://doi.org/10.1016/j.renene.2015.12.065.

[16] J.C.C. Henriques, L.M.C. Gato, J.M. Lemos, R.P.F. Gomes, A.F.O. Falcão, Peak-power control of a grid-integrated oscillating water column wave energy converter, Energy, 109, 2016, Pages 378-390, https://doi.org/10.1016/j.energy.2016.04.098.

[17] A.F.O. Falcão, J.C.C. Henriques, L.M.C. Gato, Rotational speed control and electrical rated power of an oscillating-water-column wave energy converter, Energy, vol. 120, pp. 253-261. 2017.

[18] K.M. Tsang, W.L. Chan, "An innovative approach for energy generation from waves", *Energy Conversion and Management*, vol. 92, pp. 302-311, 2015.

[19] S. Kahla, Y. Soufi, M. Sedraoui, M. Bechouat, "On-Off control based particle swarm optimization for maximum power point tracking of wind turbine equipped by DFIG connected to the grid with energy storage", in *Int. J. Hydrogen Energy* 2015, pp. 13749-13758.

[20] I. Hamzaoui, F. Bouchafaa, A. Talha, "Advanced control for wind energy conversion systems with flywheel storage dedicated to improving the quality of energy", in *Int. J. Hydrogen Energy* 2016, pp. 20832-20846.

[21] R. Pena, J. C. Clare, and G. M. Asher, “Doubly fed induction generator using back-to-back PWM converters and its application to variable-speed wind-energy generation”, *Proc. Inst. Elect. Eng.—Elect. Power Appl.*, vol. 143, no. 3, pp. 231-241, May 1996.

[22] Zhanfeng Song, Changliang Xia, Tingna Shi, Assessing transient response of DFIG based wind turbines during voltage dips regarding main flux saturation and rotor deep-bar effect, *Applied Energy*, vol. 87, pp. 3283-3293. 2010.

[23] O. Barambones, ”Sliding Mode Control Strategy for Wind Turbine Power Maximization”, *Energies*, vol. 5, no. 7, pp. 2310-2330. 2012.

[24] F.E.V. Taveiros, L.S. Barros, F.B. Costa, Back-to-back converter state-feedback control of DFIG (doubly-fed induction generator)-based wind turbines, *Energy*, vol. 89, pp. 896-906. Sep. 2015.

[25] Utkin V.I., 1993, Sliding mode control design principles and applications to electric drives, *IEEE Trans. Indus. Electro.*, **40**, 26-36.

[26] Oscar Barambones and Patxi Alkorta ”Position Control of the Induction Motor Using an Adaptive Sliding-Mode Controller and Observers”, *IEEE Trans. Ind. Electron.*, vol. 61, no. 12, pp. 6556-6465, Dec. 2014.

[27] Y. Soufi, S. Kahla, M. Bechouat, “Particle swarm optimization based sliding mode control of variable speed wind energy conversion system”, in *Int. J. Hydrogen Energy* 2016, pp. 20956-20963.

[28] Maissa Farhat, Oscar Barambones, Lassaad Sbita, A new maximum power point method based on a sliding mode approach for solar energy harvesting, *Applied Energy*, vol. 185, pp. 1185-1198. 2017.

[29] M. Alberdi, M. Amundarain, F. J. Maseda and O. Barambones, “Stalling behaviour improvement by appropriately choosing the rotor resistance value in Wave Power Generation Plants”, in *Proc. IEEE Int. Conf. on Clean Electrical Power* 2009, pp. 64-67

[30] A.J. Garrido, I. Garrido, M. Amundarain, M. Alberdi, and M. De la Sen, ”Sliding-Mode Control of Wave Power Generation Plants”, *IEEE Trans. Ind. Appl.*, vol. 48, no. 6, pp. 2372-2381, Nov./Dec. 2012.

[31] I. Garrido, Aitor J. Garrido, M. Alberdi, M. Amundarain, and O. Barambones, Performance of an Ocean Energy Conversion with DFIG Sensorless Control, Mathematical Problems in Engineering, vol. 2013, pp.1-14. 2013

[32] V. Jayashankar, K. Udayakumar B.Karthikeyan, K. Manivannan, N. Venkatraman and S. Rangaprasad, “Maximizing Power Output From A Wave Energy Plant”, in *Proc. IEEE Power Eng. Soc. Winter Meeting* 2000, vol. 3, pp. 1796-1801.

[33] Baku M. Nagai, Kazumasa Ameku, Jitendro Nath Roy, Performance of a 3 kW wind turbine generator with variable pitch control system, *Applied Energy*, vol. 86, pp. 1774-1782. 2009.

[34] Oscar Barambones, Power Output maximization for Wave Power Generation Plants using an Adaptive Sliding Mode Control, International Conference on Renewable Energy Research and Applications (ICRERA2013). Pp. 178-183. Madrid.

[35] Ying Cui, Beom-Soo Hyun, Numerical study on Wells turbine with penetrating blade tip treatments for wave energy conversion, International Journal of Naval Architecture and Ocean Engineering, vol.8, pp.456-465, 2016

[36] *SimPowerSystems 5. User's Guide*, The MathWorks

[37] Markel Penalba, José-Antonio Cortajarena, and John V. Ringwood, Validating a Wave-to-Wire Model for aWave Energy Converter—Part II: The Electrical System, Energies, vol 10, pp.1-24. 2017